A 15-year climatology of stratosphere–troposphere exchange with a Lagrangian particle dispersion model
2. Mean climate and seasonal variability

P. James,[1] A. Stohl,[1] C. Forster,[1] S. Eckhardt,[1] P. Seibert,[2] and A. Frank[2]

Received 10 June 2002; revised 12 September 2002; accepted 13 September 2002; published 8 March 2003.

[1] A comprehensive climatology of stratosphere–troposphere exchange (STE), based on 15 years of ECMWF global atmospheric reanalysis data for the period 1979–1993, has been carried out with a specially tuned version of the Lagrangian particle dispersion model, FLEXPART. The typical amplitudes, timescales, seasonality, and spatial variability of STE revealed in the climatology are described. Mean distributions of STE air masses of various ages relate to aspects of the global circulation, while anomaly patterns, such as the North Atlantic Oscillation (NAO) and El Niño, influence STE variability. Characteristic differences are seen between shallow STE flows remaining within the tropopause region (TPR) and deep STE transports, which include cases of stratospheric air reaching the lower troposphere. Unlike for shallow STE events, such deep intrusions show a distinct winter maximum. This subsequently impacts on the seasonal cycle of stratospheric ozone in the troposphere, which thus depends on altitude but also on the decay timescale of ozone. A much broader view of STE than has previously been possible is enabled. The inherent scope of STE is far wider than a discussion of cross-tropopause fluxes alone. Indeed, more than 90% of all cross-tropopause flows return within 6 hours. It is thus crucial to distinguish between short-term STE, during which air parcels rapidly recross the tropopause, and deep and/or long-term STE, in which air parcels have subsequently long residence times away from their source. *INDEX TERMS:* 0341 Atmospheric Composition and Structure: Middle atmosphere—constituent transport and chemistry (3334); 3309 Meteorology and Atmospheric Dynamics: Climatology (1620); 3334 Meteorology and Atmospheric Dynamics: Middle atmosphere dynamics (0341, 0342); 3362 Meteorology and Atmospheric Dynamics: Stratosphere/troposphere interactions

Citation: James, P., A. Stohl, C. Forster, S. Eckhardt, P. Seibert, and A. Frank, A 15-year climatology of stratosphere–troposphere exchange with a Lagrangian particle dispersion model, 2, Mean climate and seasonal variability, *J. Geophys. Res.*, *108*(D12), 8522, doi:10.1029/2002JD002639, 2003.

1. Introduction

[2] Stratosphere–troposphere exchange (STE) is an essential element of the three-dimensional global atmospheric circulation, having a central impact on atmospheric chemistry budgets in both stratosphere and troposphere. As a first approximation, STE might be considered in terms of cross-tropopause fluxes. Yet, this would be a clear oversimplification, since it does not take the subsequent paths of air masses crossing the tropopause into account, although impacts of STE depend strongly on this subsequent path. For example, when stratosphere-to-troposphere transport (here specifically referred to as STT to distinguish it from the general term STE) intrudes deeply into the troposphere, ozone-rich stratospheric air masses with high potential vorticity (PV) can be transported directly into the possibly polluted boundary layer [*Davies and Schuepbach*, 1994; *Stohl et al.*, 2000] or can trigger intense convection that may eventually lead to severe weather events [*Browning and Reynolds*, 1994; *Goering et al.*, 2001]. These parcels will eventually mix with tropospheric air and thereby contribute to the chemical budget of the troposphere. Due to the nonlinear nature of atmospheric chemistry, deep intrusions of stratospheric air that mix with lower tropospheric air have a different impact on the tropospheric chemistry budget than more shallow intrusions that only reach the upper troposphere. Thus, it is essential to distinguish between the two, if their climatologies (seasonality, geographical distribution) differ.

[3] A useful method for assessing the depth and residence times of STT (and vice versa of troposphere-to-stratosphere transport, TST) is Lagrangian particle dispersion modeling in which particles act as tracers for specific properties of the air masses they represent while being continually advected. In the first part of this paper [*James et al.*, 2003], the methodology employed with the Lagrangian particle dis-

[1]Chair of Bioclimatology and Air Pollution Research, Technical University of Munich, Freising-Weihenstephan, Germany.
[2]Institute of Meteorology and Physics, University of Agricultural Sciences, Vienna, Austria.

0148-0227/03/2002JD002639$09.00

persion model FLEXPART and some basic validation of its results was described in detail. The model was integrated over the ECMWF reanalysis data set period (ERA-15) to produce a comprehensive 15-year climatology of STE, presenting its typical magnitudes, timescales, seasonality and spatial and interannual variability. Using FLEXPART, estimates of residence times of exchange flows are limited only by the total length of the model integration itself, in this case 15 years, allowing for the first time an explicit assessment of residence times on seasonal and even longer timescales. Hence, our results compliment and extend the findings of *Sprenger and Wernli* [2003], who employ a trajectory model to examine the climatological aspects of STT and TST trajectories, traced for up to 4 days after crossing the tropopause.

[4] In this second part of the paper, the climatological results of the FLEXPART integration themselves are presented. In section 2, mean climate aspects of STE are discussed, the seasonality of the results is investigated, and the variability related to large-scale circulation anomalies is detailed. Conclusions and a summary are given in section 3.

2. Mean Climatology, Seasonality, and Variability of STE

2.1. Stratosphere-to-Troposphere Transport

[5] The mean progress of STT and TST flows intruding into the respective opposing atmospheric layers can be viewed in terms of vertical zonal mean sections of the respective species mixing ratios as a function of their age. The progress of stratospheric intrusions into the troposphere as a function of increasing age is illustrated in Figure 1 for the PV > 2 tracer, based on the annual mean. For definitions of the tracers used, as well as of other model specifics, the reader is referred to the study of *James et al.* [2003]. STT flows entering the troposphere are initially most concentrated in the subtropics near the descending branch of the Hadley circulation, which is also where the tropopause is in transition between the thermal and the dynamical definitions. There are also high concentrations of stratospheric tracer in the uppermost tropical troposphere. However, this is mostly due to shallow transports across the tropopause, as the stratospheric tracer does not descend further down in the tropical troposphere at subsequent times. Much of this STT is likely to be related to artifacts of the methodology (e.g., spatial interpolation of tropopause heights and discontinuity of tropopause heights due to the coarse resolution of the ECMWF data at tropical tropopause levels). The age spectra concept allows one to effectively filter out these events by disregarding the first few age classes, because most of the respective exchange particles return immediately to the stratosphere. On synoptic timescales, the center of action becomes focused in the midlatitudes in the middle troposphere. Much of this stratospheric air is in the form of shallow intrusions and returns to the stratosphere within synoptic timescales (Figure 1b). The more deeply intruded air, which remains, is subsequently embedded into the slower large-scale meridional circulation. On long timescales, the low-level trade wind circulations gather older stratospheric tracer gradually into the tropics where it is eventually recirculated in the tropical ITCZ into the tropopause region (TPR, defined here as the layer bounded by the PV surfaces of 1 and 4 pvu, respectively) (Figures 1e and 1f). It is seen that, on timescales of less than 4 days (Figure 1b), the impact of deep STT that reaches the Earth's surface maximizes at polar latitudes. However, for somewhat longer timescales of 4–10 days (Figure 1c) and 10–20 days (Figure 1d), the highest PV > 2 tracer surface concentrations are seen in the subtropics. It is also evident from the sequence of images in Figure 1 that the subtropical surface maximum is mostly due to quasi-isentropic descent from the middle latitudes, as the contour lines resemble the sloping isentropic surfaces. Note also the hemispheric asymmetry in these deep STT events on timescales of 4–10 and 10–20 days: The PV > 2 tracer surface concentrations maximize closer to the equator in the SH than in the NH.

[6] The equivalent vertical profiles for the PV > 4 tracer (not shown) are qualitatively similar in most aspects to those for the PV > 2 tracer. Quantitatively, however, the total tropospheric mass of young PV > 4 tracer is substantially lower than for the PV > 2 tracer. For example, only 0.3% of the mass of the troposphere is PV > 4 tracer of age less than 1 day, compared to 2.2% for the PV > 2 tracer. This means that stratospheric air originating above 4 pvu spends considerable time in the TPR before it eventually also crosses the 2 pvu surface, which acts to buffer STT. Thus, most of the air masses with stratospheric characteristics in the troposphere will have a relatively recent origin in the TPR only, and not in the stratosphere above. As the upper TPR is a mixing zone, where upwelling tropospheric air is mixed with downwelling stratospheric air [*Fischer et al.*, 2000; *Zahn*, 2001], most of the intrusions into the troposphere will have trace gas characteristics that are only partly stratospheric.

[7] To emphasize this difference and to illustrate the typical sparsity of young STT tracer in the lower troposphere, Figure 2 shows how the mean mass of the STT tracers, relative to the mass of the troposphere as a whole, increases with age at different altitudes. Note that, accumulated over all age classes, the STT tracer masses approach the total mass of the troposphere, as all tropospheric air has been in the stratosphere at some time in the past. For any given time interval, the relative mass gives the fraction of tropospheric air in the respective reservoir that was last in the stratosphere in less than this time interval. A rapid decrease with altitude of this fraction is seen for short time intervals, indicating that rapid deep STT, especially to below 3 km, does not occur frequently. At an age of 24 hours, only about 2% of the PV > 2 tracer that resides in the troposphere (itself contributing about 2% of the total tropospheric mass) is found below 3 km. By 10 days, this fraction increases to 13%. The equivalent fractions for the PV > 4 tracer are just 0.1% and 7%, respectively.

[8] Alternatively, looking at the findings with respect to the total mass of the lowest 3 km of the troposphere, only about 0.1% of the air below 3 km has been in the stratosphere, above 2 pvu, 24 hours ago, 0.7% was there 4 days ago and 3.4% 10 days ago. For a source above 4 pvu, the respective fractions for the shortest time intervals are reduced considerably (the equivalent fractions are 0.0007%, 0.05% and 0.7%, respectively), indicating that rapid deep STT from higher levels in the stratosphere is an extremely rare phenomenon. In summary, Figure 2 shows that most of the STT

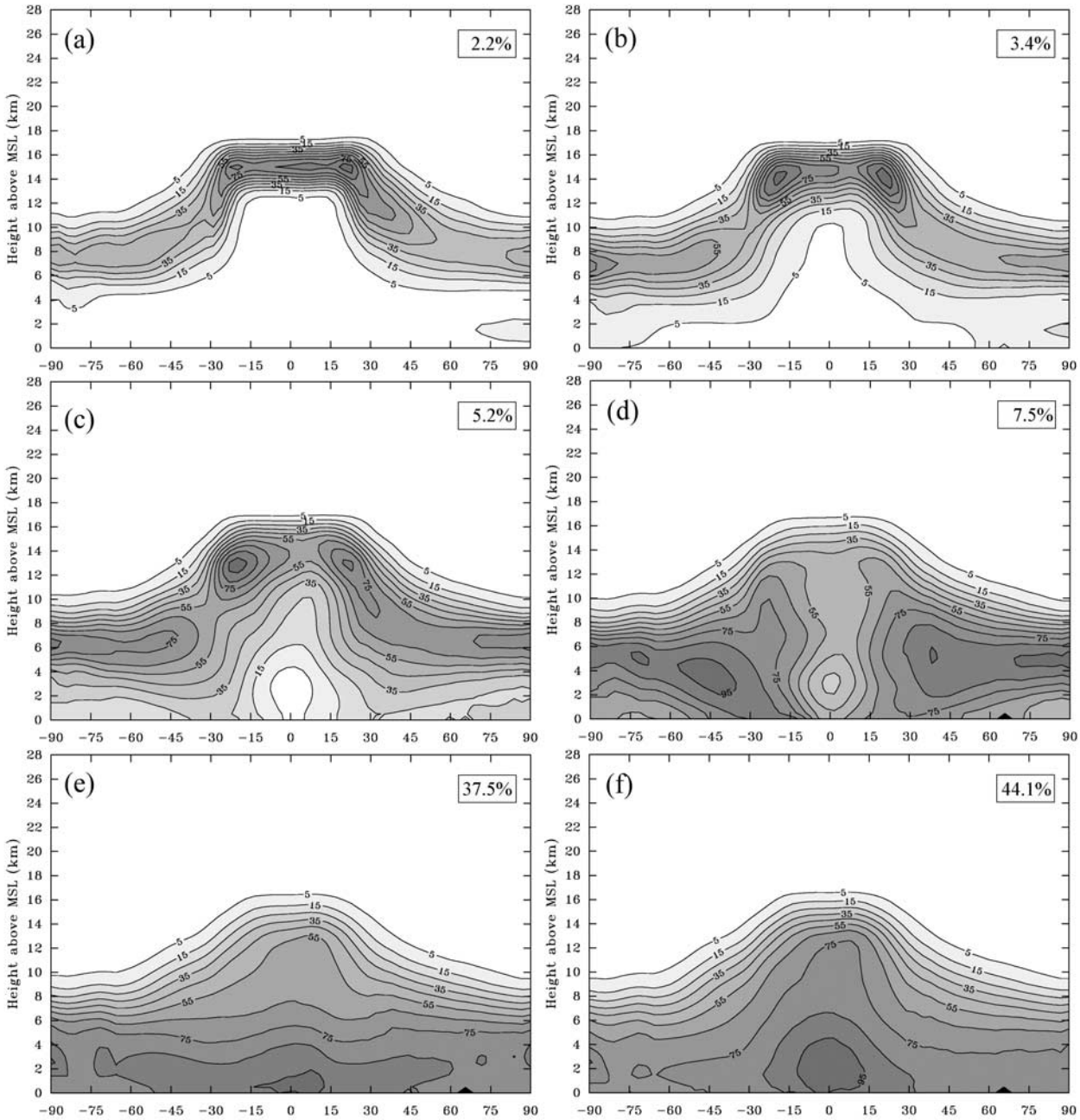

Figure 1. Latitude–height sections showing the climate mean zonal mean distributions of the stratospheric tracer (PV > 2) in the troposphere in terms of its mixing ratio as a function of age, showing (a) 0–1 days, (b) 1–4 days, (c) 4–10 days, (d) 10–20 days, (e) 20–90 days, and (f) >90 days. Contours are plotted as percentages relative to the respective maximum values. The numbers shown in the boxes show the total mass of the PV > 2 tracer in each age class group as a percentage of the average total mass of the troposphere as a whole (3.7×10^{18} kg).

events are rather shallow on short timescales, with most of the stratospheric tracer mass remaining in the upper troposphere over periods of a few days. If the tracer persists in the troposphere, it may eventually disperse to lower levels in the troposphere. Note, however, that it is the infrequent rapid deep STT events that are responsible for such important phenomena as ozone maxima at the surface, or severe weather.

[9] Looking now in more detail at rapid deep STT, it is found that such STT first reaches near the surface in the polar regions, when based on the PV > 2 tracer. However, this is primarily a reflection of the frequently low and variable polar tropopause, which is sometimes even poorly defined [*Highwood et al.*, 2000; *Zängl and Hoinka*, 2001]. When looking at the PV > 4 tracer, which excludes air sourced in the whole TPR, deep STT in the lowest 3km of

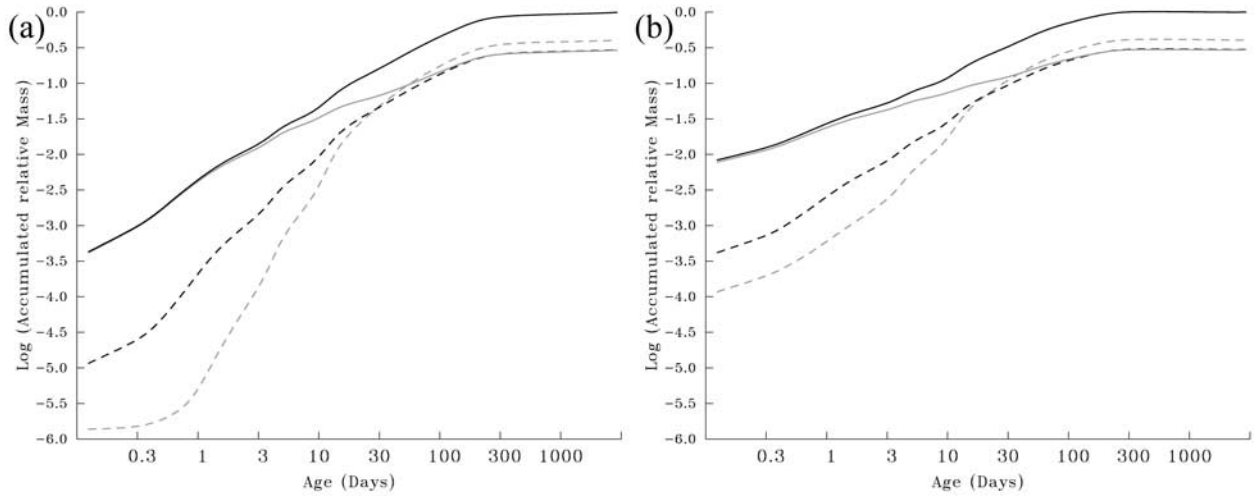

Figure 2. The global mean mass of STT tracer in the troposphere relative to the total mass of the troposphere (3.7×10^{18} kg), shown on a logarithmic scale and accumulated as a function of age class, for (a) the PV > 4 tracer and (b) the PV > 2 tracer. The black solid curve shows the total STT tracer mass in whole troposphere, while the other curves show the tracer mass in the lowest 3 km (gray dashed), the layer 3–6 km (black dashed), and the rest of the troposphere above 6 km (gray solid).

the troposphere is seen to be concentrated in midlatitudes and subtropics, even on very short timescales. As seen in Figure 1, this air descends quasi-isentropically from the middle and higher latitude stratosphere. Figure 3 now shows its climate mean horizontal distribution in terms of mixing ratios. Maxima are found especially over northern Africa and at the end of the North Pacific storm track and the start of the North Atlantic storm track in the

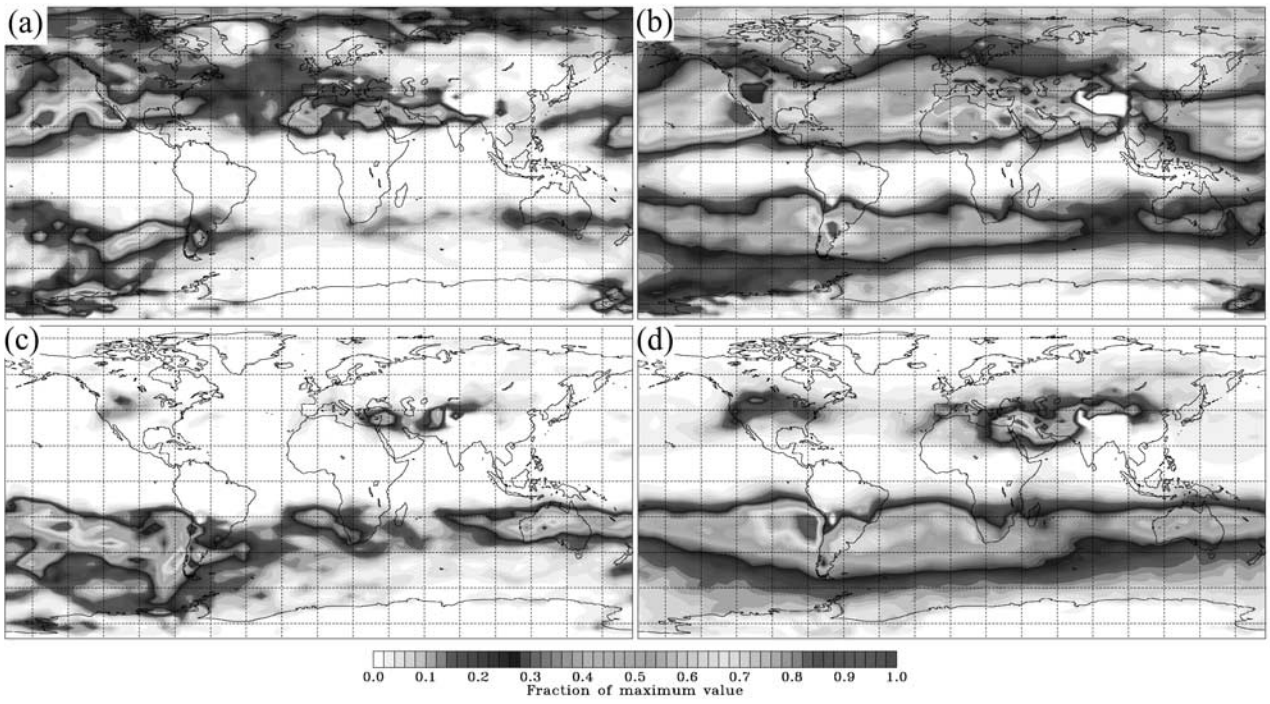

Figure 3. Latitude–longitude sections showing the climate mean mixing ratios of the stratospheric tracer (PV > 4) in the lowest 3 km (amsl) of the troposphere as a function of age (a and c) 0–4 days and (b and d) 4–10 days for (a and b) January and (c and d) July, expressed as a fraction of the respective maximum values. The equivalent total tracer masses in the lowest 3 km of the troposphere are (a) 0.7, (b) 8.9, (c) 0.4, and (d) 7.6 (each in units of 10^{15} kg), respectively, which compares to the average total mass of the troposphere of approximately 3.7×10^{18} kg. See color version of this figure at back of this issue.

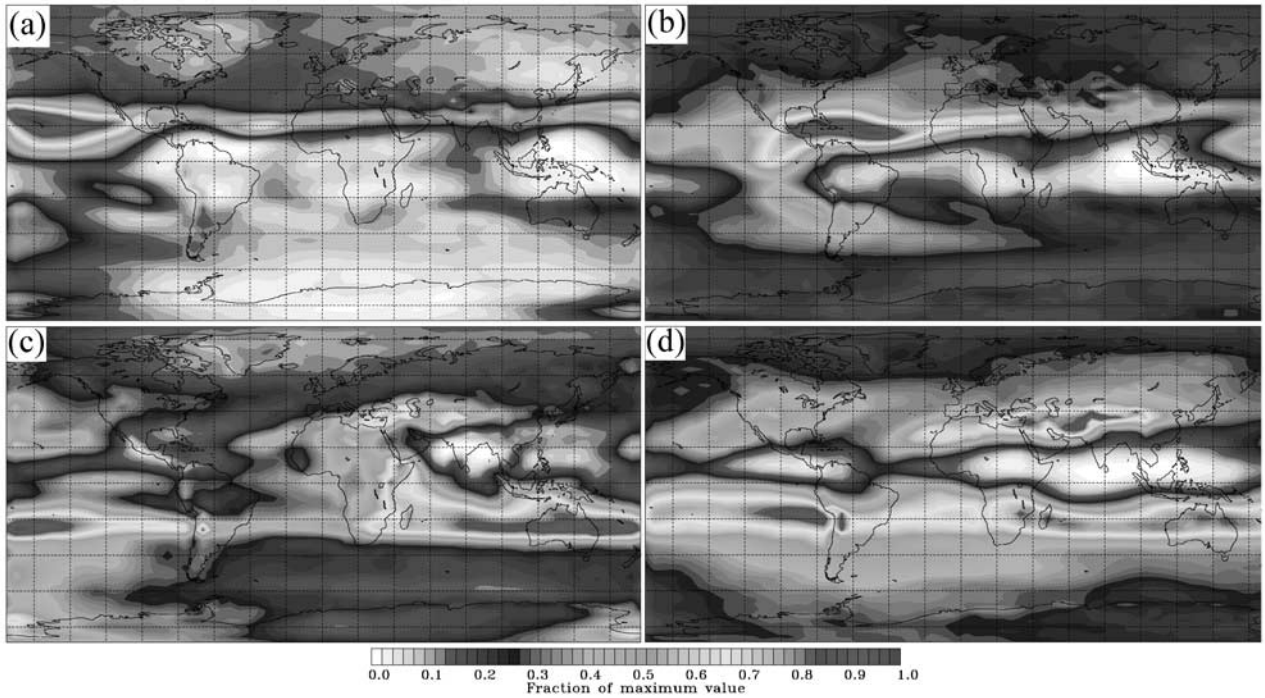

Figure 4. Latitude–longitude sections showing the climate mean mixing ratios of the stratospheric tracer (PV > 4) in the whole troposphere as a function of age (a and c) 0–4 days and (b and d) 4–10 days for (a and b) January and (c and d) July, expressed as a fraction of the respective maximum values. The equivalent total tracer masses in the whole troposphere are (a) 6.4, (b) 9.5, (c) 5.9, and (d) 9.6 (each in units of 10^{16} kg), respectively, which compares to the average total mass of the troposphere of approximately 3.7×10^{18} kg. See color version of this figure at back of this issue.

northern winter. In the northern summer, deep STT is apparently very much weaker, and the maxima shift toward the continents, which is related to the more intense convection there. These patterns compare well with the distribution of deep STT in the trajectory climatology of *Sprenger and Wernli* [2003]. In the Southern Hemisphere, the maximum regions are in the Pacific storm track to the south of the strong anticyclone west of Chile and over Australia. The seasonal cycle here is much less pronounced than it is in the Northern Hemisphere, however. The mean total mass of PV > 4 tracer in the lowest 3 km of the troposphere with ages of less than 4 days varies from 2.0×10^{14} kg in the southern summer (January) to 3.9×10^{14} kg in the southern winter (July). The equivalent figures for the Northern Hemisphere (0.4×10^{14} kg in July and 5.2×10^{14} kg in January) reveal a much larger seasonal cycle amplitude.

[10] In both hemispheres, the geographical distribution of these rapid deep STT events is very different from all STT events. In Figure 4, which shows the total columns of the 4 pvu tracer in the whole troposphere, considerably less zonal variability in the tracer distribution is seen, while there is almost no zonal variability in the STT fluxes across the tropopause (not shown).

[11] Aspects of the seasonal cycle of (deep) STT are summarized for the northern midlatitudes in Figure 5. In the upper troposphere, the seasonal cycle of STT tracer mixing ratios are relatively small, particularly for young ages. A spring maximum is found here for the PV > 4 tracer, while a winter maximum is found for the PV > 2 tracer. Nevertheless, the seasonal cycle of such shallow STT has a small amplitude, in both cases. In the lower troposphere, however, a very distinct winter maximum of STT is seen when looking at the PV > 2 tracer; the amplitude of which increases with decreasing tracer age. Note that it is mostly the seasonal differences of rapid descent in the troposphere itself [*Stohl*, 2001] that causes this strong seasonality, and not so much the differences in STT. The higher frequency of rapid descent in winter is certainly due to the intensity of baroclinic systems being greatest in wintertime. Well-developed tropopause folds and rapid deep intrusions are most likely to occur in the wake of intense (explosive) cyclogenesis, which is usually limited to the wintertime storm track regions. The seasonal cycle of the PV > 4 tracer in the lower troposphere has a weak seasonal cycle with a summer minimum for young tracer of ages of up to a day or two, while peak amplitudes shift toward the spring for older tracer. However, it is important to note that the mixing ratios of PV > 4 tracer are much smaller than those of the PV > 2 tracer, especially for ages of less than a couple of days for which the difference exceeds an order of magnitude. Thus, estimates of PV > 4 tracer amounts in the lower troposphere are likely to be rather noisy, resulting in a less reliable determination of the seasonal cycle compared to the PV > 2 tracer. The differences in the seasonal cycles of the PV > 4 and PV > 2 tracers are consistent with the descent in the lower stratosphere being more intense in spring than in winter. This is evidenced, for instance, by higher ozone concentrations in

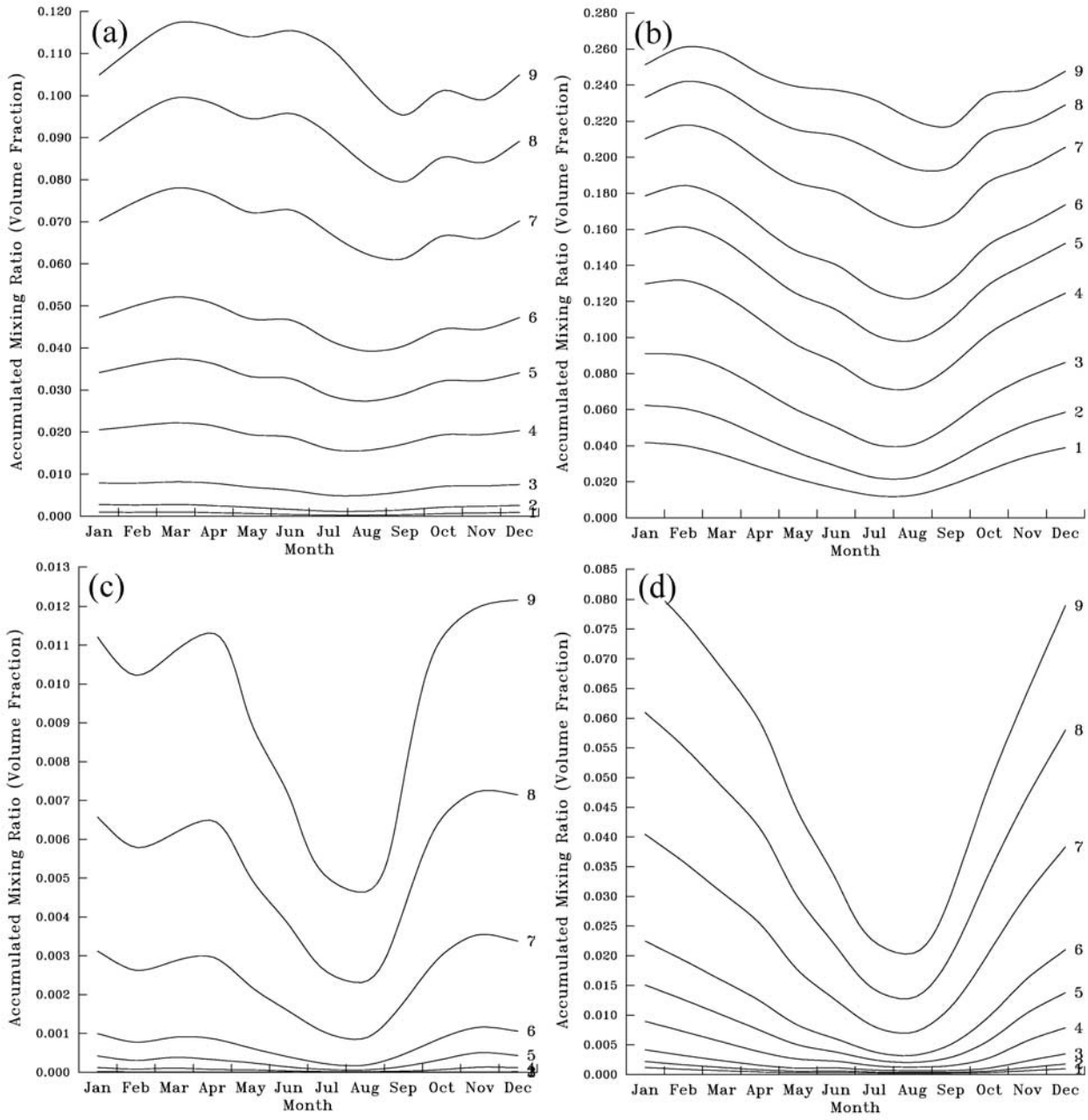

Figure 5. Mean seasonal cycle of the zonally averaged monthly mean accumulated mixing ratios of each of the first nine age classes (ages bounded upwards by 0.25, 0.5, 1, 2, 3, 4, 6, 8, and 10 days, respectively) of (a and c) the PV > 4 and (b and d) the PV > 2 stratospheric tracer in the Northern Hemisphere midlatitudes (30°–60°N) at an altitude of (a and b) 8 km amsl and (c and d) 2 km amsl.

the lower stratosphere in spring than in winter and leads to a more rapid crossing of the 2–4 pvu region.

2.2. Stratospheric Ozone in the Troposphere

[12] Ozone concentrations in the lower troposphere in the Northern Hemisphere remote from pollution sources often exhibit a late springtime (April and May) maximum [*Monks*, 2000]. Since the net mass flux of air across the extratropical tropopause also features a maximum in spring [*James et al.*, 2003], it was often concluded that the spring maximum in surface ozone is caused by STT. However, our results must cast some doubt on this simple assumption, as the seasonal cycle of the PV > 2 tracer at the surface is distinctly different from that of net STE. There are two reasons for this: first, in contrast to the net STE (i.e., STT−TST) flux across the tropopause, the gross STT flux has a late winter maximum. This is illustrated in Figure 6 showing the climate mean seasonal cycle of the gross downward cross-tropopause flux of air as a function of latitude (compare with the net STE seasonal cycle in the study of *James et al.* [2003, Figure 1]).

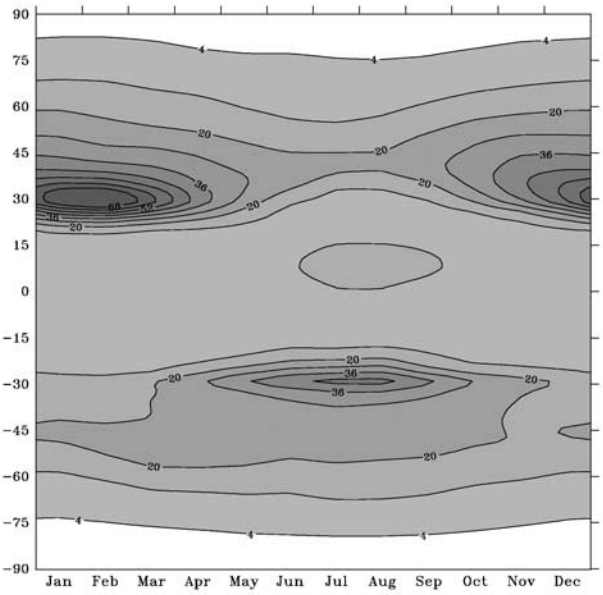

Figure 6. Mean seasonal cycle of the zonal mean gross downward cross-tropopause flux as a function of latitude in units of 10^9 kg s^{-1} deg^{-1}.

Late winter maxima are evidenced in both hemispheres. Second, rapid deep descent in the troposphere occurs most frequently in winter and decreases toward summer. For stratospheric tracer ages of less than 40 days (and even more so for younger tracer ages) this leads to an enhanced seasonal variation in stratospheric tracer concentrations at the surface, compared to that of the gross flux across the tropopause, and that in the upper troposphere.

[13] As our model does not account for chemical processes, we cannot calculate ozone budgets in the troposphere. However, global chemistry models, which are normally used for this task, have their own problems. Numerical diffusion, combined with low resolution, was identified as a major deficiency of these models, leading to overestimation of deep STT [*Meloen et al.*, 2003; *Cristofanelli et al.*, 2003]. Thus, it is worthwhile to explore some aspects of the ozone seasonal cycle in a quantitative way with our model.

[14] To investigate how the seasonal variations of STT can be expected to impact on the seasonal cycle of ozone at various altitudes in the troposphere, we prescribe a mean seasonal cycle of ozone mixing ratios for the northern midlatitudes in the lower stratosphere, using monthly values of its linear relationship with PV derived from observations [*Stohl et al.*, 2000] (Note that this overestimates stratospheric ozone to some extent, because it is assumed that all ozone above 2 pvu is of stratospheric origin. In reality, though, there will be a tropospheric contribution due to TST even above 2 pvu). The decay time constant of ozone in the troposphere is highly variable and depends strongly on sunlight and humidity levels. We test the sensitivity of our results to some different decay timescales (7, 15, and 30 days, respectively), which span typical values obtained from chemical models [*Liu et al.*, 1987]. The total stratospheric ozone contribution at various tropospheric altitudes is thus integrated over all age classes and over the PV > 2 and PV > 4 tracers, as shown in Figure 7, taking into account that the PV > 4 tracer is always contained in a subset of the PV > 2 tracer. The total ozone contribution increases strongly with increasing decay timescale. At a decay timescale of 30 days, the ozone contribution exceeds 30 ppb in the lower troposphere in winter, which is certainly too high, while the seasonal cycle maximum in March and April is fairly constant with altitude, at least up to 6 km (note that 8 km may not always be in the troposphere, especially in wintertime troughs). However, for the much shorter decay timescale of 7 days, the seasonal cycle shifts with altitude from a distinct winter maximum below 2 km to a March maximum in the middle troposphere. At all decay timescales, the annual ozone minima shift to later in the year with increasing

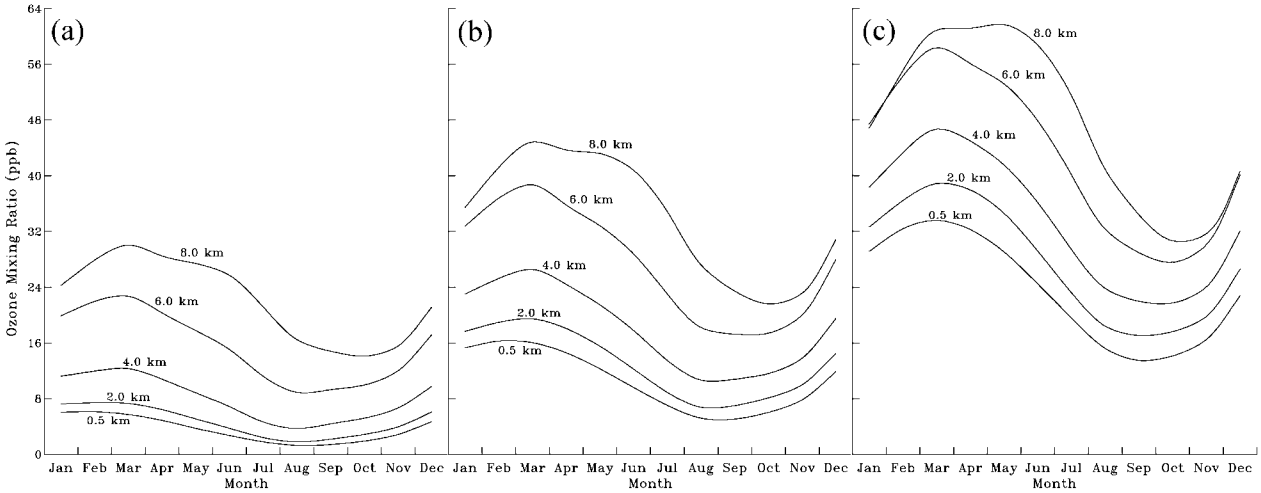

Figure 7. Mean seasonal cycle of the mixing ratio of ozone of stratospheric origin in the troposphere in the northern midlatitudes (30°–60°N) at altitudes of 0.5, 2, 4, 6, and 8 km amsl, respectively, based on assumptions of the ozone decay timescale of (a) 7 days, (b) 15 days, and (c) 30 days.

altitude, typically from August at low altitudes to October in the upper troposphere. Since the results are highly sensitive to the chosen decay time constant of ozone, we cannot settle the issue of ozone's tropospheric seasonal cycle conclusively here. However, where remote surface stations observe an annual ozone maximum as late as May, it appears highly unlikely that STT can be the major factor causing this maximum, especially since we have assumed a constant ozone lifetime, whereas in reality the lifetime decreases from winter to spring, due to increasing radiation and water vapor concentrations. This would shift the maximum STT contribution to an earlier date as we have obtained.

2.3. Mass Fluxes and Depth of STT

[15] To emphasize further the fundamentally large differences between shallow and deep STT, we show how the mass fluxes associated with STT flows across specific surfaces vary dramatically with age and vertical extent. If we first consider the gross fluxes of the PV > 2 pvu and PV < 2 pvu tracers across the tropopause (i.e., the 2 pvu surface), we can evaluate the residence time of stratospheric air in the troposphere and tropospheric air in the stratosphere. There are large upward (372.3×10^{17} kg/yr) and downward (376.7×10^{17} kg/yr) mass fluxes in the extratropical Northern Hemisphere that almost compensate each other. The annual net mass flux (4.4×10^{17} kg/yr) is a small residual of these and is directed from the stratosphere to the troposphere, in agreement with previous budget estimates [see *James et al.*, 2003 for a comparison].

[16] Such large cancellations between upward and downward gross fluxes are a common problem in flux estimates. Much of this cancellation involves transient vertical excursions on short timescales, which may result in very large instantaneous gross fluxes across some surface. Indeed, more than 90% of the PV > 2 tracer (PV < 2 tracer) in the troposphere (stratosphere) has a residence time of less than 6 hours, before returning. Note that estimates of fluxes on short timescales depend critically on model details (e.g., the interpolation of the tropopause height), whereas results for older ages are far less sensitive to changes of these details. It is found that the fluxes of PV > 2 tracer (PV < 2 tracer) that stayed more than 4 days in the extratropical Northern Hemisphere troposphere (stratosphere) are only 7.8 (4.2) $\times 10^{17}$ kg/yr, or approximately 1–2% of the total FLEXPART fluxes.

[17] Clearly, strictly cross-tropopause fluxes of air masses whose boundary is defined with the tropopause itself are a somewhat artificial measure and give no real indication about the depth of exchange. For tracer younger than 6 hours, the gross downward flux of PV > 4 air across the tropopause is more than an order of magnitude smaller than the total gross downward cross-tropopause flux (not shown), implying that nearly 95% of this total flux is of air from within the TPR itself. Thus, requiring a tracer to cross the TPR before calculating its mass flux across the lower boundary of this region acts to filter out the very shallow excursions of tracer away from its source region, which are highly sensitive to the model details. Indeed, it is found that only about 1.5% of the total instantaneous cross-tropopause mass flux can be associated with trajectories descending through the whole TPR within about 1 day.

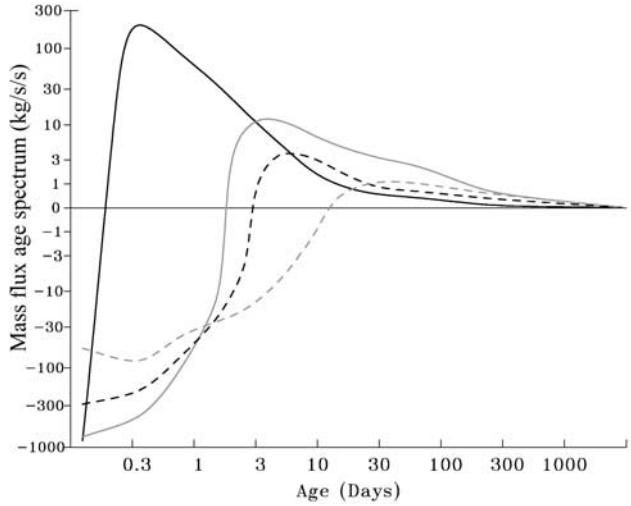

Figure 8. Age spectra of net mass fluxes in kg s^{-1} s^{-1} across various surfaces, plotted on an optimized logarithmic scale, showing the net flux of the PV > 2 tracer across the tropopause itself (black solid curve) and across the 1 pvu surface (gray solid), with the net fluxes of the PV > 4 tracer across the 2 pvu (black dashed) and 1 pvu (gray dashed) surfaces, respectively. The values are normalized by the width of the respective age classes. Net upward fluxes are positive.

[18] In Figure 8, the changes of some global mean net fluxes across the tropopause and 1 pvu surfaces with age are summarized. The large initial net flux of PV > 2 tracer down into the troposphere (note that, by definition, all downward flux of the PV > 2 tracer across the tropopause must occur in the first age class) is balanced by a net returning flux of progressively older tracer back into the stratosphere. It is a remarkable fact that this return flux of stratospheric air decays rapidly with age and already peaks in the second age class (6–12 hours), similarly to what has been found for the gross fluxes, of which more than 90% return within the first 6 hours. The net flux of the PV > 2 tracer remains downward across the 1 pvu surface for ages up to 2 days. For the PV > 4 tracer, which originates above the TPR, it takes 3 days for the net flux across the tropopause to become upwards and more than 10 days for the net flux across the 1 pvu surface to reverse sign.

2.4. Troposphere-to-Stratosphere Transport

[19] Now looking at upward transport in general, progressive upward mass fluxes are shown in Figure 9 of the boundary layer tracer. Again, the large initial net upward flux of the tracer out of the boundary layer itself is balanced by a net returning flux of progressively older tracer. The net upward fluxes of this tracer across successively higher PV surfaces become successively smaller. These latter curves each show a double peak, which moves toward older ages at higher levels. The first maximum, on very short timescales, is due to rapid convective ascent associated with (mostly subgrid scale) deep convection. The second maximum, which shifts to older ages with altitude is associated with the gradual entrainment of the boundary layer air into

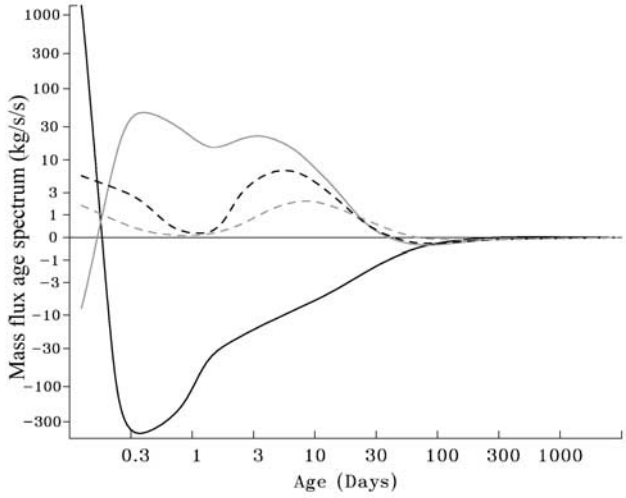

Figure 9. Age spectra of net mass fluxes in kg s^{-1} s^{-1} of the boundary layer tracer, plotted on an optimized logarithmic scale, across the top of the boundary layer itself (black solid curve), 1 pvu (gray solid), 2 pvu (black dashed), and 4 pvu (gray dashed) surfaces, respectively. The values are normalized by the width of the respective age classes. Net upward fluxes are positive.

general tropospheric air and subsequent TST flows. Note that the unexpected net downward flux for very young tracer across the 1 pvu surface is caused by this surface lying occasionally within the boundary layer itself.

[20] Looking more specifically at TST, the mean progress of tropospheric intrusions into the stratosphere as a function of increasing age is illustrated in Figure 10 for the PV < 2 tracer, based on the annual mean. The initial entrance of TST flows in the stratosphere is more uniformly spread above the whole zonal mean tropopause than is the case for STT (see Figure 1 for comparison), while the pattern also changes only very slowly with increasing age. This is certainly a result of the intrinsically high static stability of the stratosphere and the overall slow descent in the extratropical lowermost stratosphere, which hinders rapid upward transport of air masses. The uppermost stratospheric levels assessed in our study are first penetrated above the tropical convection zone, albeit typically not until ages in excess of 90 days are reached. Subsequently the tropospheric tracer is transported toward higher latitudes with the Brewer–Dobson circulation, where it descends and eventually returns to the troposphere.

2.5. Interannual Variability

[21] Since the distribution and extent of STT and TST is closely related to atmospheric circulation patterns, it can be anticipated that the year-to-year variability of STE will be correlated to atmospheric variability patterns. This has been examined empirically in our STE climatology for two major well-known circulation anomaly modes: the North Atlantic Oscillation (NAO) and the El Niño/Southern Oscillation (ENSO).

2.5.1. North Atlantic Oscillation

[22] The NAO pattern is an index of the pressure difference between Iceland and the Azores [*Barnston and Livezey*, 1987] and is the most significant and frequently recurring mode of variability across the North Atlantic. A high NAO index implies an enhanced zonal flow across the North Atlantic with well-developed storm systems taking a course toward northern Europe, resulting in wet and, in winter, warm conditions there. A low NAO index implies more disrupted flow across the Atlantic with increased meridionality, in which blocking anticyclones may develop between Iceland and northern Europe. In this case, the storm track is often weaker and less coherent and may take a more southerly course than normal.

[23] To examine systematic differences in the STE climate related to the NAO index, a new STE subclimatology was constructed from approximately one sixth of all winter months (DJF); namely those which had the largest positive NAO index deviation. A second subclimatology was produced using a further one sixth of winter months, which had the greatest negative NAO index. The latter subclimatology was then subtracted from the former to create a set of NAO+ minus NAO− fields. The actual months chosen for this analysis are listed in Table 1.

[24] In Figure 11, the anomaly patterns of stratospheric tracer in the troposphere, for ages up to 10 days, associated with NAO variability over the North Atlantic region are shown qualitatively. Between about 35°N and 55°N an increase of young PV > 2 tracer is seen at around 12 km in the positive NAO phase, relative to the negative phase. Further north, between about 60°N and 75°N and centered near 10 km altitude, a corresponding negative anomaly is seen. These anomalies relate closely to NAO-derived changes in the tropopause height over the North Atlantic, as shown by *Sprenger and Wernli* [2003] and by *Appenzeller et al.* [2000], for example. The positive NAO phase has a relatively high tropopause south of about 50°N, a strong mean meridional tropopause height gradient north of there and relatively low tropopause near 60°N; while the negative NAO phase has weak meridional tropopause height gradients and reversed height anomalies.

[25] The positive anomaly of PV > 2 tracer at near 12 km, mentioned above, subsequently descends quasi-isentropically and extends down to the surface at low latitudes when looking at older tracer between 4 and 10 days of age. This anomaly reflects the strengthened and more coherent storm track which is a feature of the positive NAO phase and which focuses STT into a narrower band.

2.5.2. El Niño/Southern Oscillation

[26] The ENSO pattern is a very large-scale oscillation of sea surface temperature (SST) anomalies in the tropical Pacific with an associated atmospheric teleconnection pattern recognized as a seesaw in the mean sea level pressure between the central Pacific (near Tahiti) and the western Pacific (near Darwin, Australia) [*Troup*, 1965]. ENSO has a very significant impact on the climate of the tropical Pacific and bordering land areas and even correlates with climate variations further afield. The largest ENSO SST anomalies occur in the tropical east Pacific where they fluctuate quasi-irregularly on a timescale of about 5 years between warm phases (El Niño) and cold phases (La Niña) [*Philander*, 1990].

[27] The primary influence of ENSO is to change the mean locations of convective activity and its amplitudes via changes in the Walker circulations over the Pacific. This in

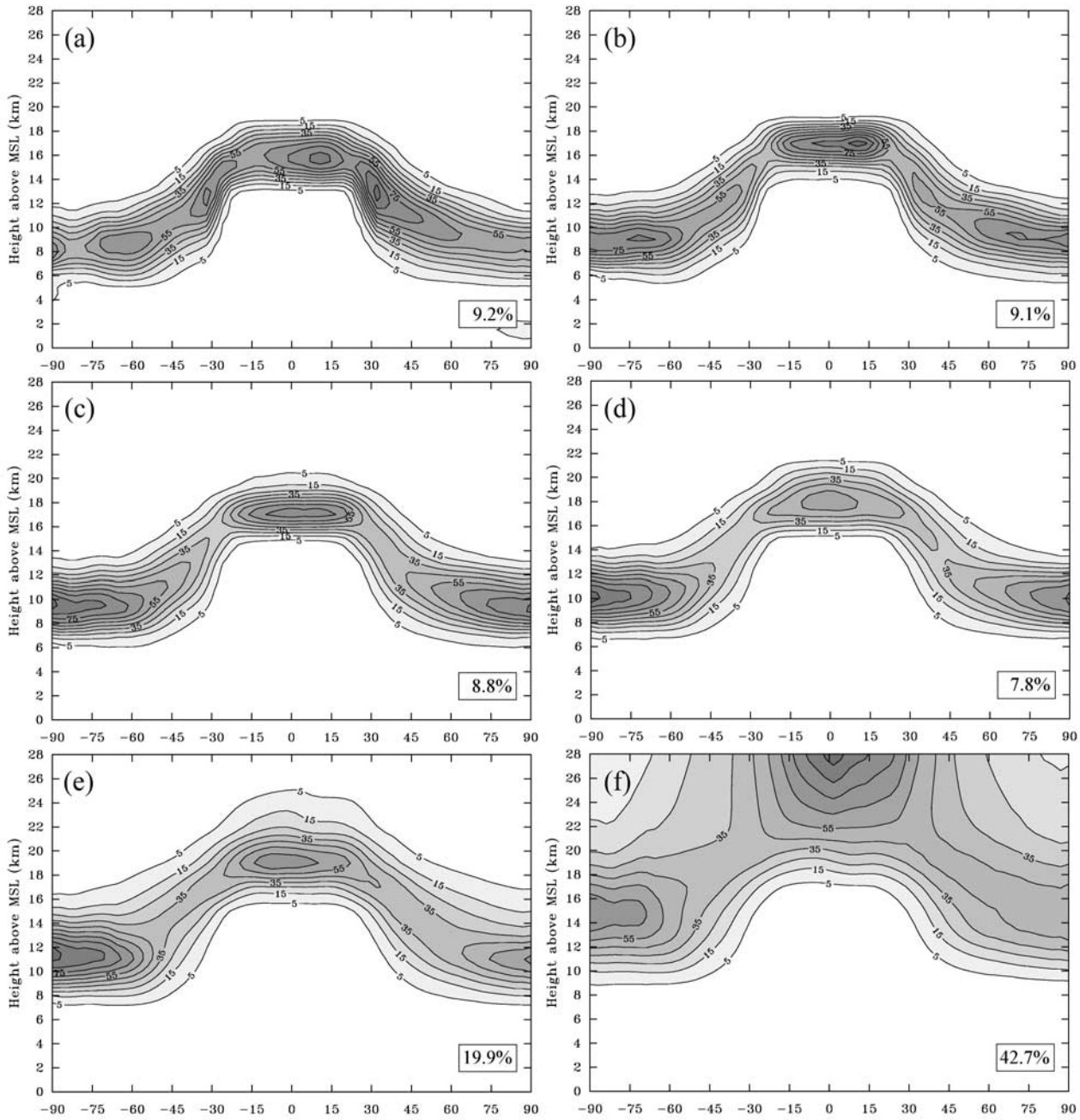

Figure 10. Latitude–height sections showing the climate mean zonal mean distributions of the tropospheric tracer (PV < 2) in the stratosphere in terms of its mixing ratio as a function of age, showing (a) 0–1 days, (b) 1–4 days, (c) 4–10 days, (d) 10–20 days, (e) 20–90 days, and (f) >90 days. Contours are plotted as percentages relative to the respective maximum values. The numbers shown in the boxes show the total mass of the PV < 2 tracer in each age class group as a percentage of the total mass of the stratosphere as a whole (6.8×10^{17} kg).

turn results in systematic changes to the tropical tropopause in this region, as shown by a diagnostic and modeling study by *Gettelman et al.* [2001], while *Hatsushika and Yamazaki* [2001] demonstrated how the region of coldest (highest) tropopause moves with the convection maximum. Here we investigate how TST distributions over the Pacific are changed by ENSO. Using a similar method to that for the NAO, Figure 12 shows tropospheric tracer mixing ratio anomalies in the lower stratosphere, separately for the western and eastern Pacific, by subtracting a subclimatology for La Niña events from one for El Niño events. During the reanalysis period, three major El Niño and two La Niña events occurred. In each case, we have defined a central 12-month period for the respective event, based on the period when the ENSO-related SST anomalies were largest. These periods are listed in Table 2.

Table 1. List of Months Used in the NAO-Related STE Subclimatology

NAO+	NAO−
February 1981	January 1980
December 1982	January 1982
January 1984	January 1985
February 1984	February 1986
January 1986	January 1987
February 1989	February 1987
December 1993	December 1987
	December 1989

[28] The El Niño minus La Niña fields show a clear upward shift of PV < 2 tracer mixing ratios above the tropopause over the eastern Pacific where the El Niño leads to enhanced and more penetrant convective activity and an increase in the tropopause height. With increasing age, this greater penetration reaches still higher altitudes. In the western Pacific where convection is relatively suppressed during El Niño, TST is significantly reduced on timescales of up to 10 days, as is anticipated. Yet, for older tracer with ages up to 90 days, TST mixing ratios become enhanced during El Niño over the western Pacific, which at first sight might seem contradictory. However, it must be remembered that the ENSO-related changes in convective activity have a higher amplitude over the eastern Pacific than over the western Pacific. This is confirmed by looking at domain averaged RMS mixing ratio anomalies. For ages up to 10 days, the RMS anomaly over the eastern Pacific of 3.1% (volume fraction in percent) is about twice that over the western Pacific of 1.6%. For older tracer of up to 90 days of age, the RMS anomaly decreases to 1.9% over the eastern Pacific, but increases over the western Pacific to 2.1%. Hence, the enhanced levels of older TST tracer over the western Pacific are probably related to tracer, which has been advected from the anomalous convection regions in the eastern Pacific by the Walker circulation.

3. Discussion and Conclusions

[29] A comprehensive study of STE, based on 15 years of ECMWF global atmospheric reanalysis data, has been undertaken with a specially tuned version of the Lagrangian particle dispersion model, FLEXPART. The goal of this work has been to produce a detailed climatology of STE, showing its typical amplitudes, timescales, seasonality and spatial and temporal variability, focussing in particular on deep and long-lasting exchange.

[30] In part 1, the model setup and the experiment methodology employed, in which a large number of particles are traced permanently and globally, allowing various age properties and pathways of air masses to be assessed on a very wide range of timescales, was described in detail. Then, in order to provide a solid foundation for discussing the STE climatology in this paper, aspects of net mass fluxes and distributions with respect to tracer age were validated against other results in the literature. The model integration was shown to have performed as anticipated, yielding statistics that compare well with other studies.

[31] In this paper, aspects of the STE climatology itself have been presented. In many ways, this work can been seen as a complimentary and parallel study to the findings of *Sprenger and Wernli* [2003], who employed a trajectory model to examine the climatological aspects of STE trajectories, also based on the same 15-year reanalysis data. Their investigation differs from our study in a number of ways and, for this reason, it is of particular value to compare the results. Sprenger and Wernli limited their study to the Northern Hemisphere, whereas the FLEXPART output has been assessed globally. Moreover, they traced STE trajectories for up to 4 days only, whereas the particle clocks in FLEXPART count indefinitely and thus can also account for

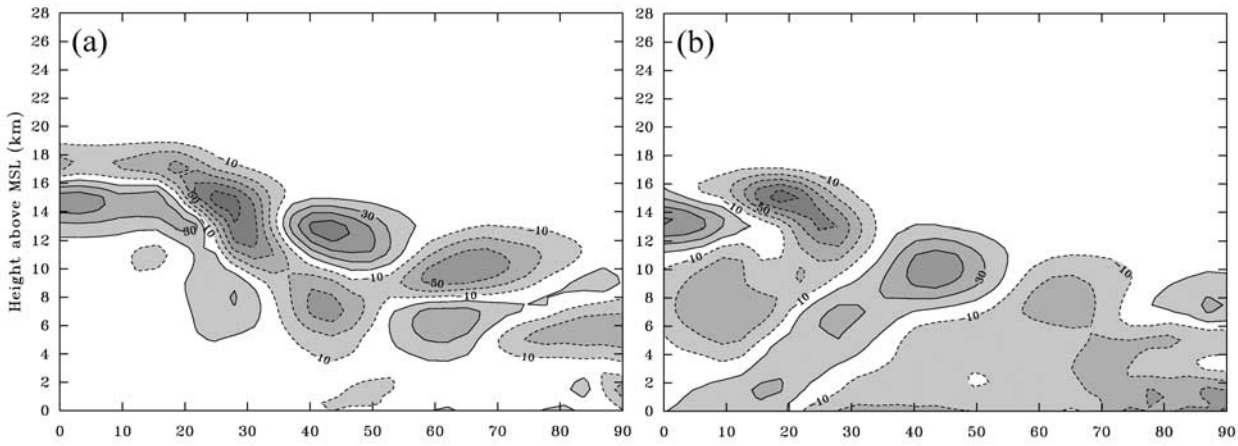

Figure 11. Latitude–height sections showing qualitatively the distribution anomaly patterns, zonally averaged between 78°W and 12°E, of the stratospheric tracer (PV > 2) in the troposphere, relating to the NAO (the mean state during the seven northern winter months with the largest positive NAO index minus the mean state during the eight winter months with the largest negative NAO index) for ages (a) 0–4 days and (b) 4–10 days. Contours are plotted as percentage changes relative to the respective maximum absolute anomaly values, and negative contours are dashed.

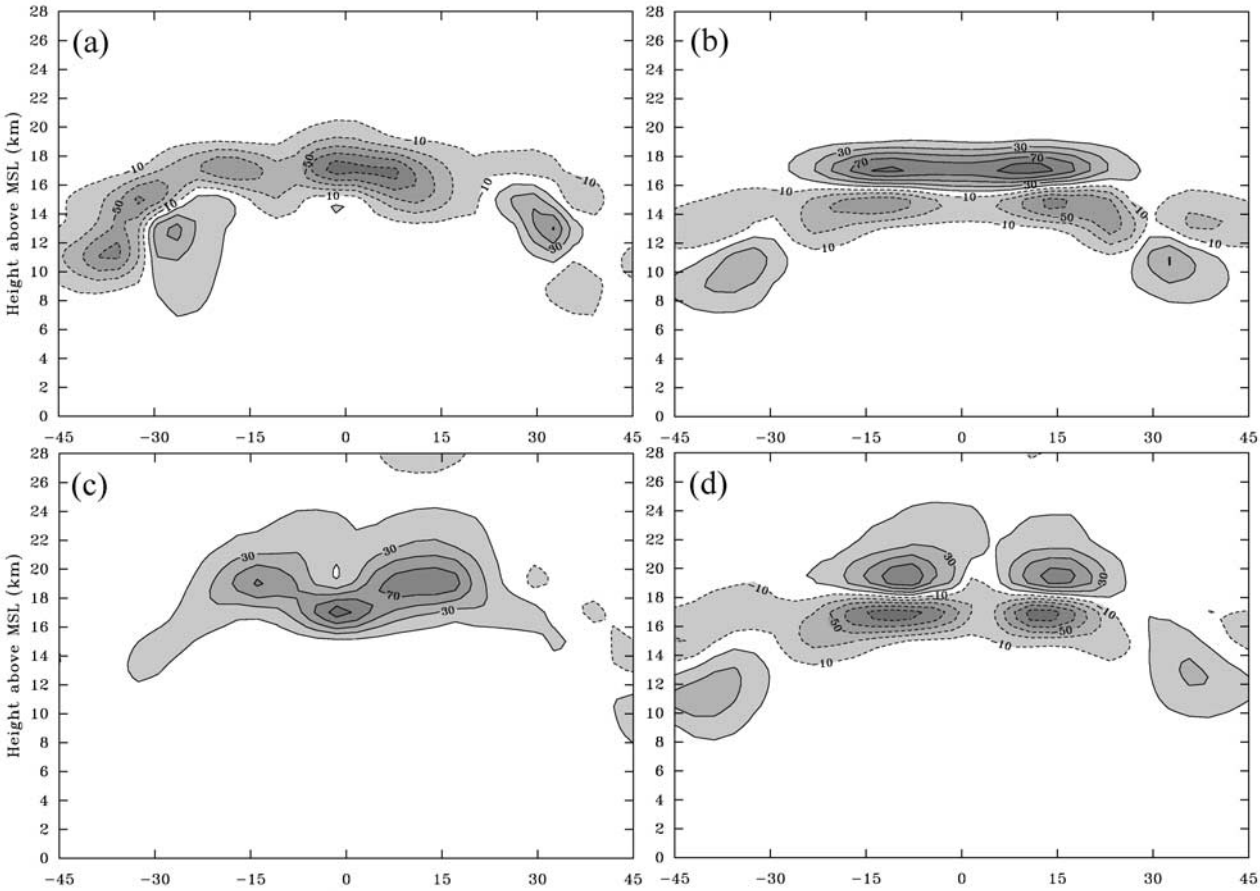

Figure 12. Latitude–height sections showing qualitatively the zonal mean distribution anomaly patterns of the tropospheric tracer (PV < 2) in the stratosphere, relating to the El Niño phenomenon (the mean state during three major El Niño events (1982–1983, 1987, and 1991–1992) minus the mean state during two major La Niña events (1984–1985 and 1988–1989)) over (a and c) the western tropical Pacific (122°E to 178°W) and (b and d) the eastern tropical Pacific (148°–88°W) for ages (a and b) 0–10 days and (c and d) 10–90 days. Contours are plotted as percentage changes relative to the respective maximum absolute anomaly values, and negative contours are dashed.

very long residence times, limited only by the total length of the integration. On the other hand, Sprenger and Wernli explicitly store the exact paths of all air mass trajectories which cross the tropopause, whereas FLEXPART only stores a derivative of this information relating to mass fluxes across specified surfaces and concentration field snapshots in conjunction with tracer age. In particular, in spite of having five different tracers in our model, the ''origin destination'' concept of STE trajectories introduced by Sprenger and Wernli is not possible with FLEXPART. Hence, in general, the two studies compliment each other well.

[32] Vertical profiles of the zonally averaged mean progress of direction-specific TST and STT flows as a function of their age have been shown (Figures 1 and 10). The initial entrance of TST flows in the stratosphere is more uniformly spread above the whole zonal mean tropopause than is the case for STT. This is certainly a result of the intrinsically high static stability of the stratosphere and the overall slow descent in the extratropical lowermost stratosphere, which hinders rapid upward transport of air masses. The uppermost stratospheric levels assessed in our study (23–27 km above local orography) are first penetrated above the tropical convection zone, albeit typically not until ages in excess of 90 days are reached. Subsequently the tropospheric tracer is transported toward higher latitudes with the Brewer–Dobson circulation, where it descends and eventually returns to the troposphere.

[33] STT flows entering the troposphere are initially most concentrated in the subtropics and in the uppermost tropical troposphere, although much of this is in the form of shallow transports across the tropopause, for little stratospheric tracer descends further down into the troposphere at sub-

Table 2. List of Months Used in the ENSO-Related STE Subclimatology

El Niño	La Niña
August 1982 to July 1983	October 1984 to September 1985
January–December 1987	April 1988 to March 1989
July 1991 to June 1992	

sequent times, especially not in the tropics. Of more significance, the center of action becomes focused in the midlatitudes in the middle troposphere on synoptic timescales. Even here, much of this stratospheric air is in the form of shallow intrusions and returns to the stratosphere within synoptic timescales. The more deeply intruded air, which remains, is subsequently embedded into the slower large-scale meridional circulation. On long timescales, the low-level trade wind circulations gather older stratospheric tracer gradually into the tropics where it is eventually recirculated in the tropical ITCZ into the TPR.

[34] It is found that only about 2% of the mass of the troposphere is composed of stratospheric air which was last in the stratosphere less than 1 day ago. Of this small fraction, only around 2% is to be found at altitudes below 3 km. The amount of young stratospheric tracer generally decreases rapidly with decreasing altitude, indicating that rapid deep STT does not occur frequently. Equally significant is the result that, for a stratospheric source above 4 pvu, i.e., above the TPR as a whole, just 0.0007% of the mass of the lowest 3 km of the troposphere is composed of such stratospheric air less than 1 day old, indicating that rapid deep STT from higher levels in the stratosphere is an extremely rare phenomenon. Most STT events are in fact rather shallow on short timescales, with most of the stratospheric tracer mass remaining in the upper troposphere over periods of a few days. If the tracer persists in the troposphere, it may eventually disperse unspectacularly to lower levels in the troposphere.

[35] The climate mean distribution of deep STT tracer, originating above the TPR, has been calculated in the lowest 3 km of the troposphere. Deep STT is concentrated in midlatitudes and subtropics. Maxima are found especially over northern Africa and at the end of the North Pacific storm track and the start of the North Atlantic storm track in the northern winter. In the northern summer, deep STT is apparently very much weaker and the maxima shift toward the continents, which is related to the more intense convection there. These patterns compare well with the distribution of deep STT in the trajectory climatology for the Northern Hemisphere of *Sprenger and Wernli* [2003]. In the Southern Hemisphere, the maximum regions are in the Pacific storm track to the south of the strong anticyclone west of Chile and over Australia. The seasonal cycle over the Northern Hemisphere is as much as 5 times larger in amplitude than in the Southern Hemisphere.

[36] The mean seasonal cycle of midlatitude STT has a very weak amplitude in the upper troposphere, but becomes more and more pronounced at progressively lower altitudes. Rapid deep STT has a strong maximum centered toward the late winter, in good agreement with the seasonal cycles computed by *Sprenger and Wernli* [2003]. The impact of the seasonal cycle of STT on lower tropospheric ozone concentrations has been assessed with an empirical model based on our STT statistics. This allows us to test whether STT is a likely cause of the late springtime ozone maximum which observational evidence has pointed to for ozone concentrations in the lower troposphere in the Northern Hemisphere remote from pollution sources. The results are seen to be highly sensitive to the chosen decay time constant of ozone, and this question cannot be settled conclusively here. However, whereas remote surface stations observe an annual ozone maximum as late as May, STT appears at best to be capable of explaining an seasonal ozone peak in the lower troposphere no later than about March.

[37] Mass fluxes associated with STT flows across specific surfaces have been computed and vary dramatically with age and vertical extent. Net mass fluxes are often found to be the residual of very large gross fluxes on short timescales. More than 90% of all cross-tropopause fluxes return within 6 hours, implying that a large proportion of cross-tropopause mass fluxes are transient and shallow in nature. Indeed, it is found that only about 1.5% of the total instantaneous cross-tropopause mass flux can be associated with trajectories descending through the whole TPR within about 1 day.

[38] Changes to some aspects of the STE climatology relating to two well-known large-scale circulation anomaly patterns, NAO and ENSO, have been assessed and discussed qualitatively. The frequency of occurrence and location of STT over the North Atlantic correlates with the NAO index due to the associated changes in storm track position and intensity. Similarly, El Niño events lead to anomalously strong convective activity over the eastern Pacific in the tropics which, in turn, is evidenced in enhanced TST air masses in the lower stratosphere which are subsequently redistributed westward in the Walker circulation.

[39] This study has presented a much broader view of STE than has previously been possible. The inherent scope of STE is revealed to be far greater than that provided by a discussion limited merely to cross-tropopause fluxes. It is crucial to distinguish between transient, shallow exchange, in which air parcels rapidly recross the tropopause, and deep and/or long-term exchange transports, in which air parcels have subsequently long residence times away from their source, possibly impacting on atmospheric chemistry budgets.

[40] **Acknowledgments.** This research has been carried out as part of the STACCATO project (influence of Stratosphere–Troposphere Exchange in a Changing Climate on Atmospheric Transport and Oxidation Capacity) funded by the European Commission under contract EVK2-1999-00316 as part of the Fifth Framework Programme. The ECMWF and the German Weather Service (DWD) are also gratefully acknowledged for giving us access to the reanalysis atmospheric data sets. We thank the STACCATO community, particularly H. Wernli, for valuable discussions.

References

Appenzeller, C., A. K. Weiss, and J. Staehelin, North Atlantic Oscillation modulates total ozone winter trends, *Geophys. Res. Lett.*, *27*, 1131–1134, 2000.

Barnston, A. G., and R. E. Livezey, Classification, seasonality and persistence of low-frequency atmospheric circulation patterns, *Mon. Weather Rev.*, *115*, 1083–1126, 1987.

Browning, K. A., and R. Reynolds, Diagnostic study of a narrow cold-frontal rainband and severe winds associated with a stratospheric intrusion, *Q. J. R. Meteorol. Soc.*, *120*, 235–257, 1994.

Cristofanelli, P., et al., Stratosphere to troposphere transport: A model and method evaluation, *J. Geophys. Res.*, *108*(D12), doi:10.1029/2002JD002600, in press, 2003.

Davies, T. D., and E. Schuepbach, Episodes of high ozone concentrations at the surface resulting from transport down from the upper troposphere/lower stratosphere: A review and case studies, *Atmos. Environ.*, *28*, 53–68, 1994.

Fischer, H., et al., Tracer correlations in the northern high latitude lowermost stratosphere: Influence of cross-tropopause mass exchange, *Geophys. Res. Lett.*, *27*, 97–100, 2000.

Gettelman, A., W. J. Randell, S. Massie, F. Wu, W. G. Read, and J. M. Russell III, El Nino as a natural experiment for studying the tropical tropopause region, *J. Clim.*, *14*, 3375–3391, 2001.

Goering, M. A., W. A. Gallus Jr., M. A. Olsen, and J. L. Stanford, Role of stratospheric air in a severe weather event: Analysis of potential vorticity and total ozone, *J. Geophys. Res.*, *106*, 11,813–11,823, 2001.

Hatsushika, H., and K. Yamazaki, Interannual variations of temperature and vertical motion at the tropical tropopause associated with ENSO, *Geophys. Res. Lett.*, *28*, 2891–2894, 2001.

Highwood, E. J., B. J. Hoskins, and P. Berrisford, Properties of the Arctic tropopause, *Q. J. R. Meteorol. Soc.*, *126*, 1512–1532, 2000.

James, P., A. Stohl, C. Forster, S. Eckhardt, P. Seibert, and A. Frank, A 15-year climatology of stratosphere–troposphere exchange with a Lagrangian particle dispersion model, part 1, Methodology and validation, *J. Geophys. Res.*, *108*(D12), doi:10.1029/2002JD002637, in press, 2003.

Liu, S. C., et al., Ozone production in the rural troposphere and the implications for regional and global ozone distributions, *J. Geophys. Res.*, *92*, 4191–4207, 1987.

Meloen, J., et al., Stratosphere–troposphere exchange: A model and method intercomparison, *J. Geophys. Res.*, *108*, doi:10.1029/2002JD002600, in press, 2003.

Monks, P. S., A review of the observations and origins of the spring ozone maximum, *Atmos. Environ.*, *34*, 3545–3561, 2000.

Philander, S. G. H., *El Nino, La Nina and the Southern Oscillation*, 289 pp., Academic, San Diego, Calif., 1990.

Sprenger, M., and H. Wernli, A northern hemispheric climatology of cross-tropopause exchange for the ERA15 time period (1979–1993), *J. Geophys. Res.*, *108*(D12), doi:10.1029/2002JD002636, in press, 2003.

Stohl, A., A 1-year Lagrangian "climatology" of airstreams in the Northern Hemisphere troposphere and lowermost stratosphere, *J. Geophys. Res.*, *106*, 7263–7279, 2001.

Stohl, A., et al., The influence of stratospheric intrusions on alpine ozone concentrations, *Atmos. Environ.*, *34*, 1323–1354, 2000.

Troup, A. J., The Southern Oscillation, *Q. J. R. Meteorol. Soc.*, *91*, 490–506, 1965.

Zahn, A., Constraints on 2-way transport across the Arctic tropopause based on O_3, stratospheric tracer (SF_6), and water vapor isotope (D, T) tracers, *J. Atmos. Chem.*, *39*, 303–325, 2001.

Zängl, G., and K. P. Hoinka, The tropopause in the polar regions, *J. Clim.*, *14*, 3117–3139, 2001.

S. Eckhardt, C. Forster, P. James, and A. Stohl, Chair of Bioclimatology and Air Pollution Research, Technical University of Munich, Am Hochanger 13, D-85354, Freising-Weihenstephan, Germany. (james@forst.tu-muenchen.de)

A. Frank and P. Seibert, Institute of Meteorology and Physics, University of Agricultural Sciences, Vienna, Austria.

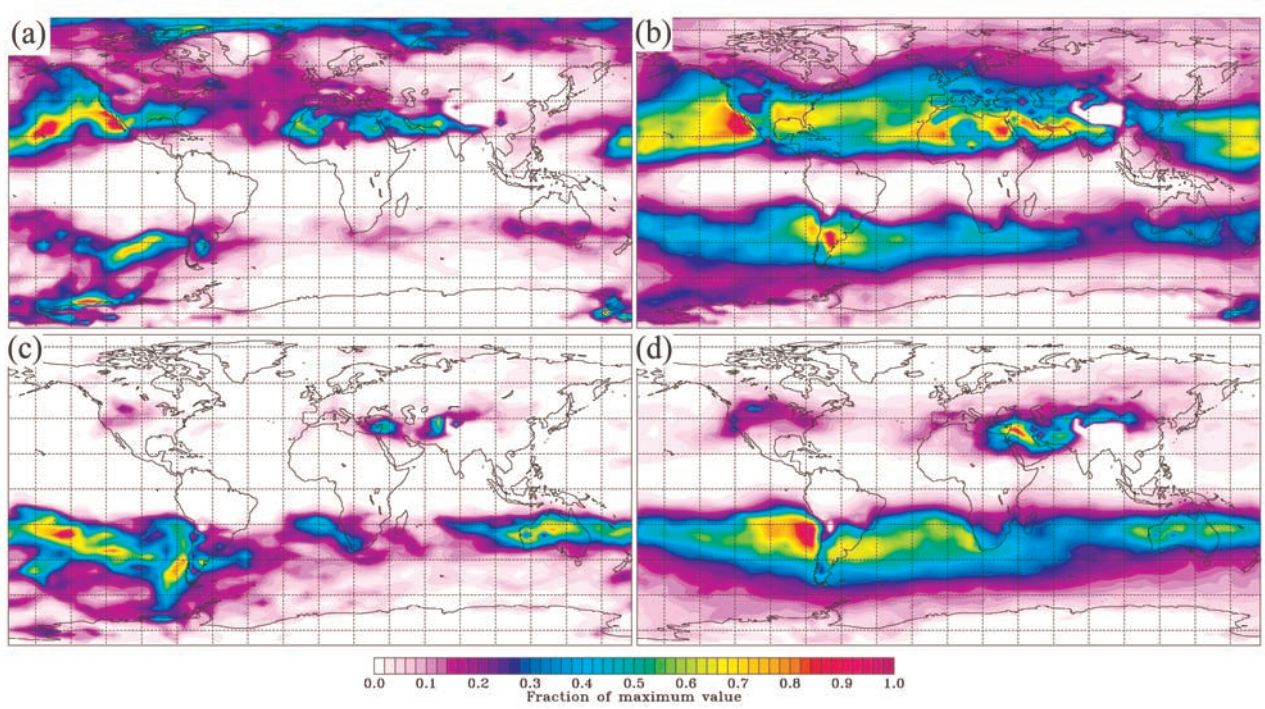

Figure 3. Latitude–longitude sections showing the climate mean mixing ratios of the stratospheric tracer (PV > 4) in the lowest 3 km (amsl) of the troposphere as a function of age (a and c) 0–4 days and (b and d) 4–10 days for (a and b) January and (c and d) July, expressed as a fraction of the respective maximum values. The equivalent total tracer masses in the lowest 3 km of the troposphere are (a) 0.7, (b) 8.9, (c) 0.4, and (d) 7.6 (each in units of 10^{15} kg), respectively, which compares to the average total mass of the troposphere of approximately 3.7×10^{18} kg.

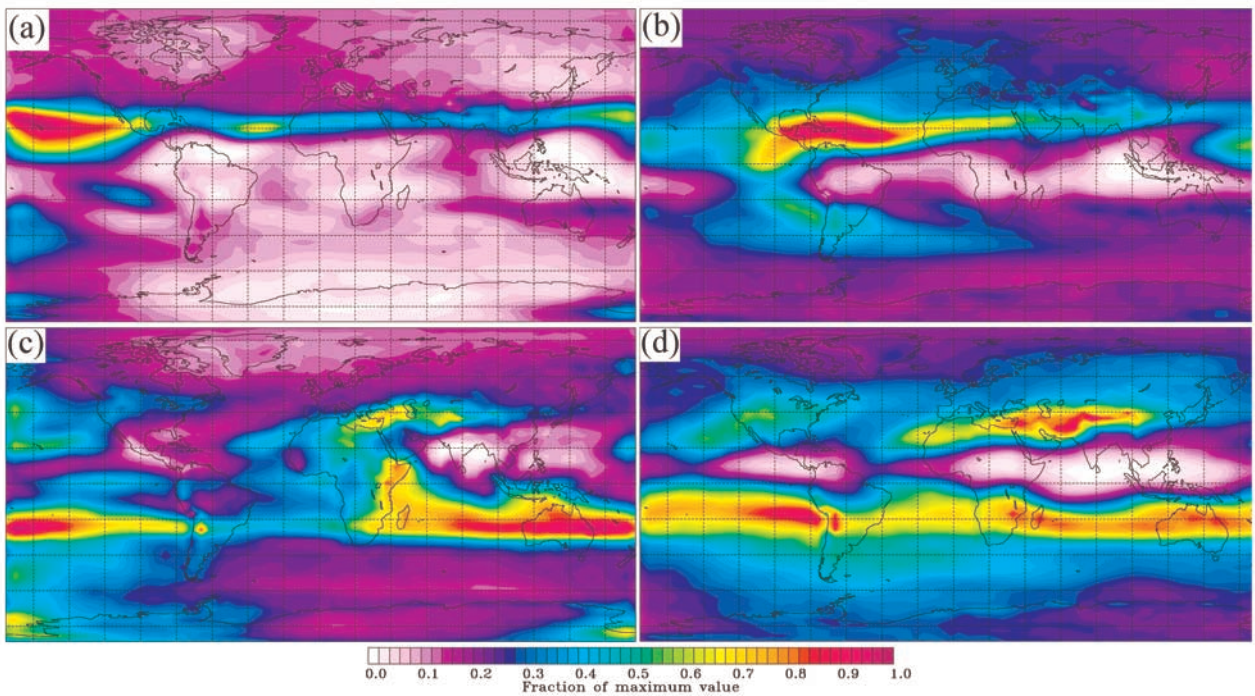

Figure 4. Latitude–longitude sections showing the climate mean mixing ratios of the stratospheric tracer (PV > 4) in the whole troposphere as a function of age (a and c) 0–4 days and (b and d) 4–10 days for (a and b) January and (c and d) July, expressed as a fraction of the respective maximum values. The equivalent total tracer masses in the whole troposphere are (a) 6.4, (b) 9.5, (c) 5.9, and (d) 9.6 (each in units of 10^{16} kg), respectively, which compares to the average total mass of the troposphere of approximately 3.7×10^{18} kg.